Journal of Applied Electrochemistry (2022) 52:477–486
https://doi.org/10.1007/s10800-021-01653-y

RESEARCH ARTICLE

Spherical and core–shell-structured $LiMn_{1.5}Ni_{0.5}O_4$ lithium-ion battery cathode with enhanced cyclability

Muharrem Kunduraci[1] · **Uğur Çağlayan**[2]

Received: 21 September 2021 / Accepted: 24 November 2021 / Published online: 6 January 2022

Abstract

Spherical $LiMn_{1.5}Ni_{0.5}O_4$(LMN) spinel materials with Co or Al doping were synthesized using coprecipitation technique and the dopants' impacts on cathode performance were explored. While both dopants were conducive to the capacity retention of LMN spinel, aluminum was more effective. Cobalt doping also helped increase the discharge capacity of control spinel, unlike aluminum. Core–shell-structured materials with Co-doped core and Al-doped shell segments were synthesized with the aim to create synergy between two dopants. Indeed, the best cathode performance in terms of lithium capacity and cyclability was reached with core–shell material. The best cathode material denoted as CS 3-1 had a first cycle lithium capacity of 133.1 mAh g^{-1} and exhibited capacity fade rate of 0.08% per cycle. X-ray diffraction and FTIR studies revealed that all cathode materials were single phase and spinel type with Fd3m space group. Focused-ion beam (FIB) and Scanning Electron Microscope photos showed that spinel materials were made of distinct spherical particles 3–4 μm in diameter. The core–shell structure was also substantiated with the photos. Energy dispersive analysis confirmed that constituent elements Mn, Ni, Co and Al had a homogeneous distribution within spherical particles. Electrochemical impedance spectroscopy results showed that Al doping on the surface was beneficial to reducing impedance growth, thereby explaining the better cyclability and rate performance of these cathodes.

Graphical abstract

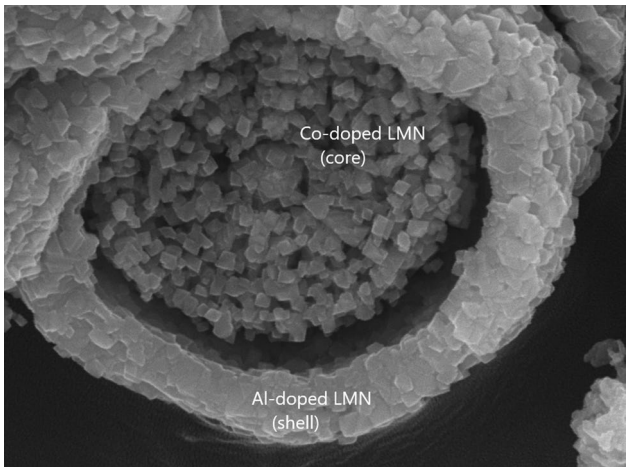

Keywords Battery · Spinel · Coprecipitation · Core · Shell

✉ Muharrem Kunduraci
kunduraci.m@hotmail.com

Extended author information available on the last page of the article

1 Introduction

Lithium-ion batteries are the most widely adopted electrochemical energy storage technology. They are expected to maintain their lead over other battery technologies in the future thanks to their long cycle life, specific energy and power densities. Ni and Co-heavy cathode materials such as $LiNi_{0.8}Co_{0.1}Mn_{0.1}O_2$, $LiNi_{1/3}Co_{1/3}Mn_{1/3}O_2$ (NMC) and $LiNi_{0.8}Co_{0.15}Al_{0.05}O_2$ (NCA) dominate the electric vehicle and portable electronics sectors as they offer high energy densities with excellent cycling stability [1–5]. However, the production costs of batteries are bound to rise due to escalating price increases in nickel and cobalt ores in the past years. On the other hand, manganese is one of the cheapest elements used in lithium-ion batteries and Mn-based cathode materials constitute a good alternative to above mentioned cathodes. Spinel-type $LiMn_{1.5}Ni_{0.5}O_4$ (LMN) is the most promising one in this group of materials and has been extensively studied in the last decade [6–8]. Thanks to its high operating voltage of 4.7 V and theoretical gravimetric capacity of 147 mAh g^{-1}, its specific energy density of 690 Wh kg^{-1} can rival those of NMC and NCA battery materials. Despite its low cost, easy synthesis and high energy density, LMN has not been used in a commercial product so far since its cyclability does not extend beyond a few hundred cycles, with the situation getting much worse when the cell operates above 50 °C [9, 10].

A few reasons have been suggested in the past to explain the origin of poor cycling stability. They included oxidation of electrolyte above 4.3 V and subsequent formation of an insulating layer on spinel particle surface, degradation of surface layer of spinel particles due to attack from hydrofluoric acid and metal dissolution into liquid electrolyte. The remedies to deal with such mechanisms included engineering of surface chemistry with dopants [11–14], coating of spinel material with a thin layer of passive oxides [15–21], altering the microstructure of active material to control its interaction with liquid electrolyte [22, 23] and using electrolyte additives to control the thickness and chemical composition of cathode-electrolyte interface [24, 25].The common idea in all these measures might be related to protecting cathode surface against harmful reactions with organic electrolyte. The surface coating techniques using wet chemistry or a vapor phase deposition lack practicality and are not suitable for mass production yet. The addition of electrolyte additives might cause undesirable effects on the anode side and needs extensive experimentation. On the other hand, the use of dopants whether in the bulk or on the surface is a much more feasible option as the addition of small amount of dopant does not require modification of existing synthesis method.

Several dopants including Co [26], Cr [27], Al [28], B [29], Mg [30], Fe [31], Si [32], Mo [33], Ti [34] and Zr [35] have been shown to enhance the cycling stability and rate performance of $LiMn_{1.5}Ni_{0.5}O_4$ cathode material. Even dual-doping strategy with Cu-Al [36], Mg-Y [37], Mg-Si [38], Cr-Nb [39] and Ti-La [40] couples were utilized to create synergy between different elements. However, a core–shell structure where the bulk and the shell of $LiMn_{1.5}Ni_{0.5}O_4$ spinel material is doped by different elements has not been reported so far to the best of our knowledge.

In this study, we experimented with Co and Al doping of $LiMn_{1.5}Ni_{0.5}O_4$ both individually and in combination. Cobalt element was chosen for the core of spinel cathode since it is electrochemically active around 4.7 V similar to nickel, thereby not hurting the specific capacity of the cathode material. As for the shell component, aluminum element was selected since it is well known to have a positive role in the capacity retention of $LiMn_{1.5}Ni_{0.5}O_4$ and other cathode materials [41, 42]. Coprecipitation synthesis technique was chosen to produce spinel cathode materials as it is well suited to control the distribution of various elements from core to surface. This advantage enables researchers to prepare core–shell structures with different characteristics. Our initial battery tests showed that Co doping into LMN ($LiMn_{1.5}Ni_{0.45}Co_{0.05}O_4$) was helpful to boost discharge capacity while Al doping ($LiMn_{1.475}Ni_{0.475}Al_{0.05}O_4$) had a positive impact on capacity retention in line with our earlier expectations. A core–shell structure having synergetic coupling of Co-doped bulk and Al-doped shell exhibited the best performance in terms of capacity, cyclability and rate capability.

2 Experimental

2.1 Preparation of metal carbonate precursors

In order to prepare $LiMn_{1.5}Ni_{0.5}O_4$ (LMN), $LiMn_{1.5}Ni_{0.45}Co_{0.05}O_4$ (LMNC) and $LiMn_{1.475}Ni_{0.475}Al_{0.05}O_4$(LMNA) cathodes, their precursor materials of $Mn_{0.75}Ni_{0.25}CO_3$, $Mn_{0.75}Ni_{0.225}Co_{0.025}CO_3$ and $Mn_{0.735}Ni_{0.24}Al_{0.025}CO_3$ were initially synthesized by coprecipitation technique. A total of 0.02 mol of metal sulfate or nitrate salts ($MnSO_4{\cdot}H_2O$, $NiSO_4{\cdot}6H_2O$, $CoSO_4{\cdot}7H_2O$, $Al(NO_3)_3{\cdot}9H_2O$) was dissolved in deionized (DI) water. The final volume was adjusted to 10 mL (solution A). In another solution, 2.72 g of $Na_2CO_3{\cdot}H_2O$ (=0.022 mol) was dissolved in DI water with the final volume again brought to 10 mL (solution B). 100 mL of DI water was poured in a 400 mL beaker (solution C) and its temperature was raised to 40 °C. Once the temperature of solution C stabilized, solution A and B were added into solution C simultaneously at a feeding rate of 0.16 mL min^{-1}. The solution was stirred

at 800 rpm at all times to avoid settling of particles to the bottom. After both solutions were consumed, stirring continued for 4 more hours to produce spherical particles until the final diameter reached 3–4 µm. Later, precursor particles were sieved and rinsed with 1 L of DI water and put into drying oven at 120 °C overnight. Core–shell materials were prepared using the same procedures with the exception that solution A was split into two parts. The first core–shell material was synthesized by adding first a total of 0.15 mol of Mn, Ni and Co salts into solution C followed by a total of 0.05 mol of Mn, Ni and Al salts (CS 3-1). For the second core–shell material, 0.10 mol of each solutions was used (CS 1-1). After the carbonate precursors were fully dried, they were mixed with required amount of Li_2CO_3 and heated to 730 °C in air for 10 h to obtain crystalline spinel materials. In total, five spinel materials were produced (LMN, LMNA, LMNC, CS 3-1 and CS 1-1) and analyzed.

2.2 Electrode preparation and electrochemical testing

In order to prepare positive electrodes, 200 mg of active material, 25 mg of Timcal Super C45 conductive carbon, 25 mg of Polyvinylidene fluoride and 1.5 g of N-Methyl-2-pyrrolidone (NMP) solvent were put inside a vial. After magnetically stirring the mixture for 1 h at 500 rpm, about 20 mg of the slurry was cast onto pre-cleaned 1 cm^2 Aluminum foil. The slurry was dried by removing the solvent at 120 °C overnight. The active material loading ended up to be about 2 mg cm^{-2}. 2032 type coin cells were prepared in an Argon-filled glovebox with H_2O and O_2 levels under 1 ppm. The cells contained 1 M $LiPF_6$ in EC-DMC electrolyte, Lithium counter electrode and Whatman glass fiber paper separator. The cells were charged and discharged at a constant current density of 50 mA g^{-1} (*C*/3) between 3.0 and 4.9 V vs. Li metal for 80 cycles. For rate study, fresh cells were discharged four times at *C*/3, 1*C*, 3*C*, 6*C* and *C*/3 in sequence. Following the end of rate study, electrochemical impedance spectroscopy analyses of coin cells were performed by applying 10 mV of AC voltage at fully discharged states.

2.3 Material characterization

Phase analysis of spinel materials was performed using PANalytical Empyrean X-ray diffractometer using CuK_α radiation. The diffraction patterns were gathered between $2\theta = 10°$ and 70° using a scan rate of 2° min^{-1}. Infrared spectroscopy (Jasco FT/IR-6700) was utilized to determine the space group of spinel materials. The morphological features of precursor and spinel materials were investigated with Quanta 200 model field emission scanning electron microscope (FESEM) operated at 20 kV. Energy dispersive spectroscopy (EDS) attached to ZEISS Supra 55 FESEM was used for elemental mapping. For Inductively Coupled Plasma-Mass Spectroscopy (ICP-MS) measurements, the precursor materials were initially dissolved in a mixture of HNO_3 and HCl acids under heating and pressure. After full dissolution of solid materials, the analysis was carried out with NEXION 2000 P (Perkin Elmer).

3 Results

The X-ray diffraction patterns of all five spinel materials are plotted in Fig. 1a. All of the major peaks can be assigned to $LiMn_{1.5}Ni_{0.5}O_4$ phase with JCPDS Number of 80-2162. However, two small peaks around 33° and 56° can be noticed in CS 3-1 spinel. These peaks were assigned to Li_2O, which probably resulted from the decomposition of unreacted Li_2CO_3 during calcination step. Another small peak around 16° in CS 1-1 remains unidentified.

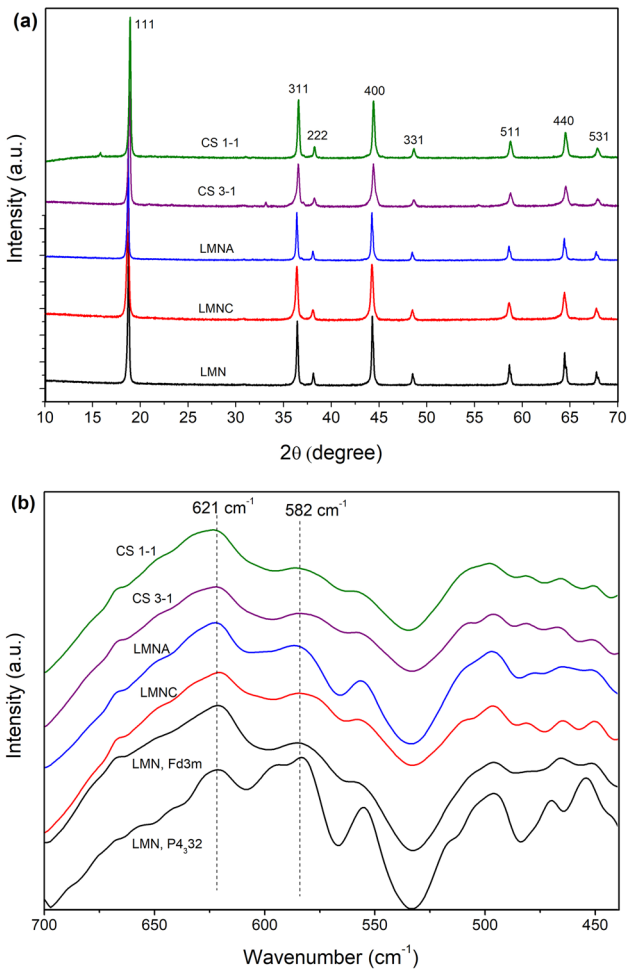

Fig. 1 **a** X-ray diffraction spectra of five spinel materials and **b** their FTIR profiles

$LiMn_{1.5}Ni_{0.5}O_4$ is known to adopt two different space groups, namely cation ordered $P4_332$ and disordered $Fd3m$, depending on material composition, synthesis temperature and ambient oxygen pressure during heat treatment [43–46]. There are plenty of studies in literature that demonstrated that Fd3m outperforms $P4_332$ in terms of cyclability and high rate performance [47–49]. In order to rule out the role of space group among our materials, Fourier transformed infrared spectra (FTIR) of all materials were collected to identify the available phase and displayed in Fig. 1b. For comparison, FTIR spectrum of a $P4_332$ spinel is also provided. The ratio of two peaks at 621 cm^{-1} and 582 cm^{-1} was used previously as an indicator to distinguish two phases [43, 50]. It is seen clearly that all five spinels belong to Fd3m space group and space group will not be a factor in comparing their electrochemical performance.

The morphological features of spinel materials were studied using scanning electron microscope (SEM). The photos of cathode samples that belong to LMN, LMNA and LMNC spinels are shown in Fig. 2a–c. All particles are spherically shaped and have an average diameter of 3–4 µm. The tetrahedra-shaped primary crystals peculiar to spinel structure are noticed on the surface of LMN and LMNC samples. The surfaces of these samples also appear porous. On the other hand, the outer surface of LMNA seems denser and smoother (Fig. S1). In order to reveal the distribution of metals within particles, energy dispersive spectroscopy (EDS) analyses were performed on metal carbonate precursors of LMNA and LMNC materials. The mapping results are shown in Fig. 3. The Mn, Ni, Co and Al elements can be seen to be distributed homogeneously within the particles with no sign of segregation, thereby indicating the success of coprecipitation synthesis.

SEM photos of core–shell-structured CS 3-1 and CS 1-1 spinels after high-temperature annealing step (i.e., 730 °C) were also taken and depicted in Fig. 2d–i. In Fig. 2d and e, CS 3-1 spinel consists of spherical particles 4 µm in diameter with narrow size distribution. Based on 3 to 1 mol ratio of LMNC and LMNA used in the synthesis of this material, the thickness of shell layer is calculated to be about 5% of overall particle diameter (Fig. S2). A thin layer with a thickness of about 200 nm can be noticed on the outer surface of cracked particle. This number is consistent with the thickness of a potential LMNA shell layer (i.e., 1/22 of overall diameter). In order to better visualize this layer, a cross-section view of spherical particle was generated

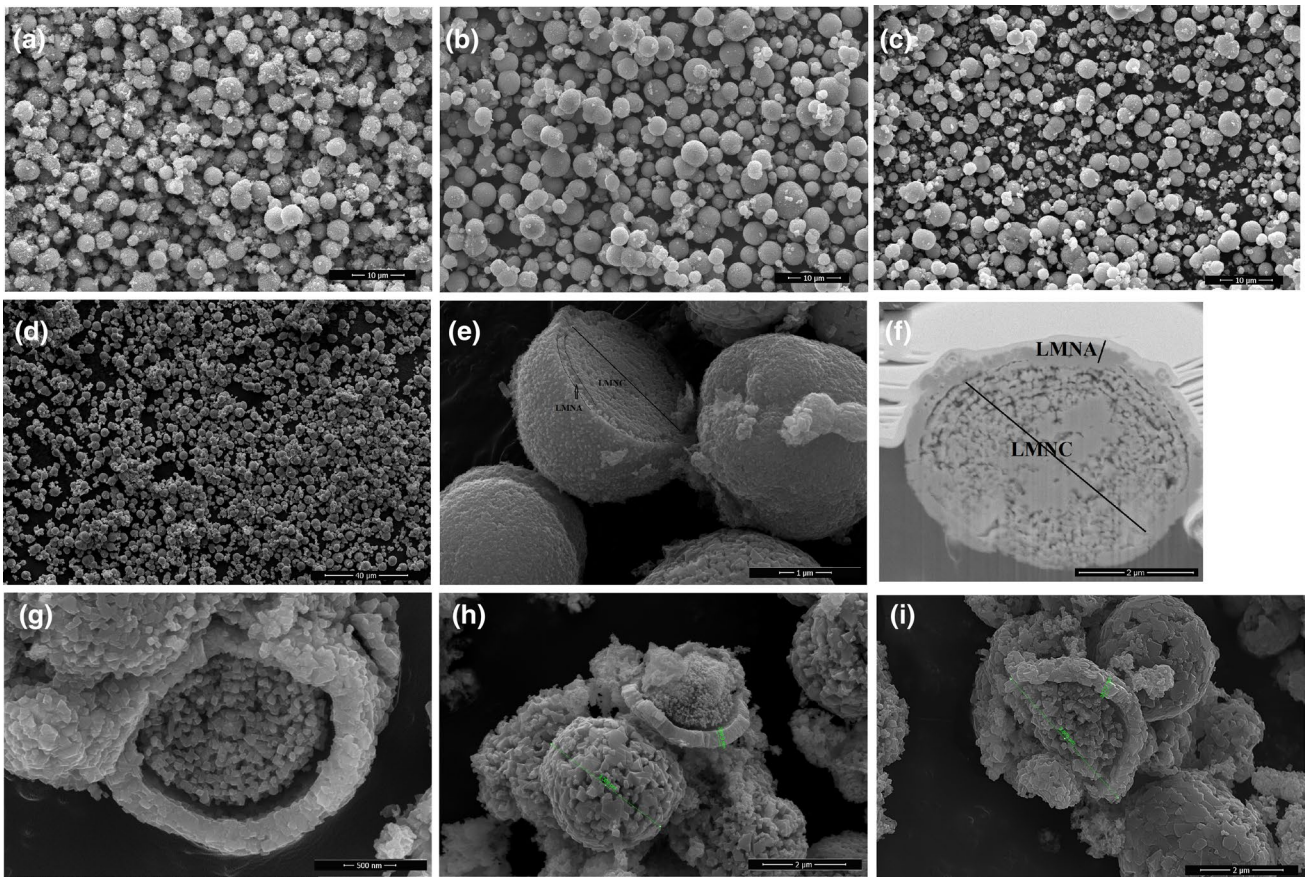

Fig. 2 SEM photos of spinel samples that belong to **a** LMN, **b** LMNC, **c** LMNA, **d–f** CS 3-1 and **g–i** CS 1-1

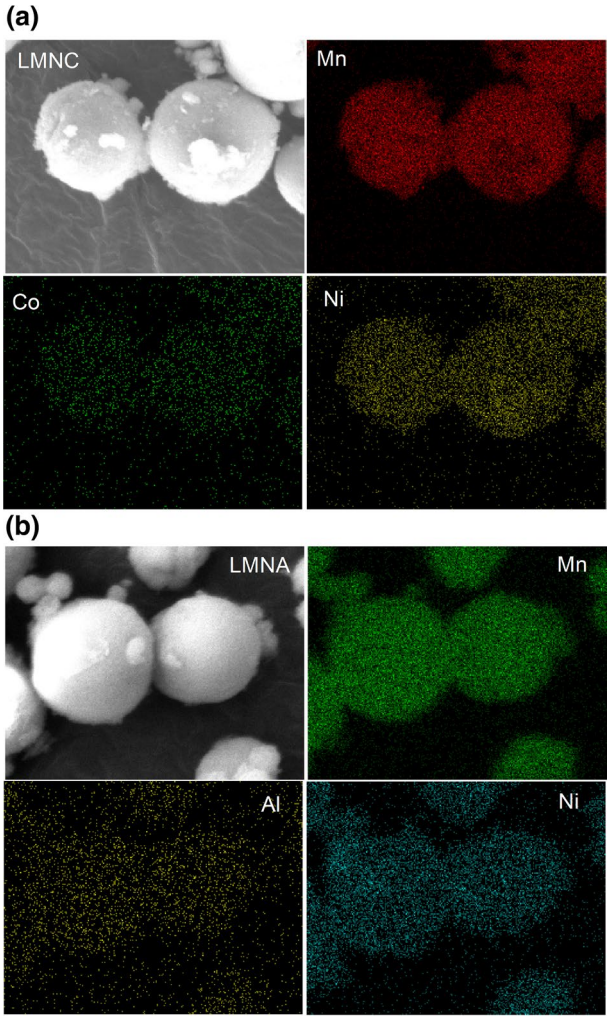

Fig. 3 EDS elemental mappings of metal carbonate precursors belonging to **a** LMNC and **b** LMNA spinels

using Focused-ion Beam (FIB) technique. The image from this analysis is given in Fig. 2f. The core of the sample is composed of 50–100 nm in diameter individual particles coalesced together during coprecipitation synthesis. Small pores can be observed in the core, thereby suggesting that the high-temperature annealing step did not result in appreciable fusion of smaller particles. On the other hand, there is a discernible shell layer reaching a thickness of 200 nm, indicating that core–shell structure was not destroyed after high-temperature heat treatment. This value agrees well with previous SEM photo, supporting the argument that a core–shell structure indeed exists. As a final note, this shell layer seems to lack any porosity as opposed to the core of the particle, highlighting the good contrast between LMNC and LMNA layers.

In order to study the impact of core–shell ratio on battery performance, CS 1-1 spinel with thicker shell layer was synthesized as well. Since the mole ratio of core LMNC to shell LMNA was 1, the thickness of shell layer is calculated to be 10% of particle diameter (Fig.S2). The SEM images of CS 1-1 heat treated at 730 °C are shown in Fig. 2g–i. The photos with broken particles were intentionally chosen to view and distinguish core–shell structure. The spinel particles are spherical and 3–4 μm in diameter. An excellent contrast between core and shell sections is easily noticed again. The shell layers, similar to CS 3-1, seem to be dense unlike porous core segment. Also, as expected, the shell thickness is about 300–400 nm and corresponds to 1/10 of overall diameter. This observation is in excellent match with thickness calculations.

The elemental compositions of five spinels were measured using ICP-MS method. Table 1 includes the starting compositions and ICP-MS measurement results. The concentrations of Mn, Ni and Co elements are within 5% of originally targeted values, thereby exhibiting good chemistry control. On the other hand, the percentage of Al is about half of intended numbers. However, the fact that Al deficiency is present in all samples makes direct comparison of LMNA, CS 1-1 and CS 3-1 spinels possible.

The lithium capacity of spinels and the redox reactions were determined by applying constant charge and discharge currents between 3.5 and 4.9 V vs. Li metal. The voltage profiles of all spinels in the first cycle are plotted in Fig. 4. All cathodes exhibit electrochemical activity around 4.1 V and 4.7 V regions. The activity within 4.1 V and 4.3 V range is due to $Mn^{3+} \leftrightarrow Mn^{4+}$ redox couple [51, 52]. Even though the starting compositions of spinels were charge balanced to avoid Mn^{3+}, the appearance of Mn^{3+} in the final spinel lattice still took place due to oxygen loss from spinel during high-temperature annealing. The activity in high voltage section is attributed to $Ni^{2+} \leftrightarrow Ni^{4+}$ transitions [52]. As

Table 1 ICP-MS elemental analyses results of five spinel materials

Name of cathode sample	Chemical composition of cathode sample	ICP-MS results			
		Mn	Ni	Co	Al
LMN	$LiMn_{1.5}Ni_{0.5}O_4$	1.496	0.504	–	–
LMNC	$LiMn_{1.5}Ni_{0.45}Co_{0.05}O_4$	1.466	0.479	0.055	–
LMNA	$LiMn_{1.475}Ni_{0.475}Al_{0.05}O_4$	1.488	0.488	–	0.024
CS 1-1	0.5 × LMNC + 0.5 × LMNA	1.477	0.475	0.035	0.013
CS 3-1	0.75 × LMNC + 0.25 × LMNA	1.479	0.466	0.048	0.007

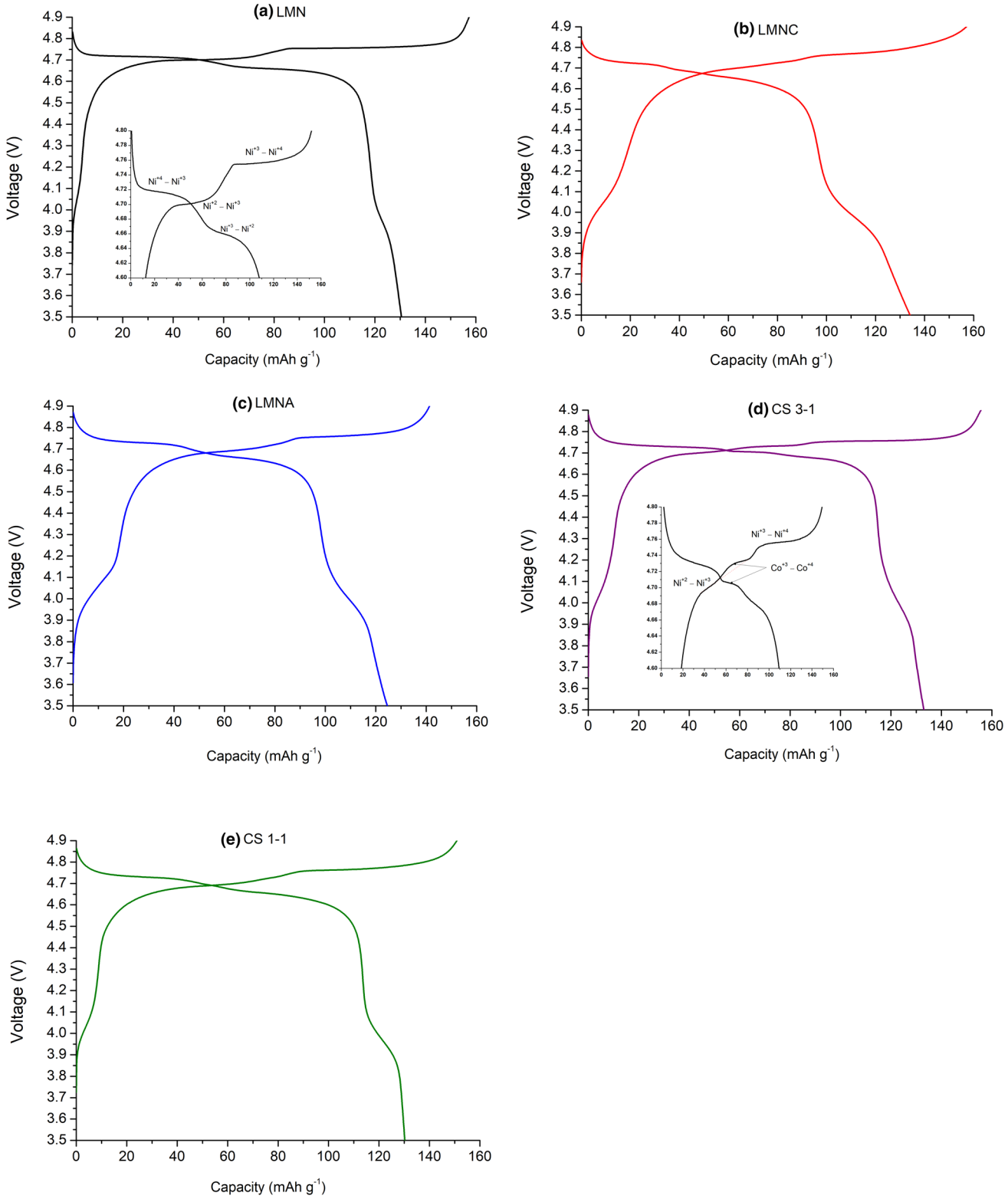

Fig. 4 First cycle charge and discharge voltage profiles of five spinel cathodes: **a** LMN, **b** LMNC, **c** LMNA, **d** CS 3-1 and **e** CS 1-1

shown clearly in the inset of LMN spinel, this transition happens in two steps; namely $Ni^{2+} \leftrightarrow Ni^{3+}$ below 4.70 V line and $Ni^{3+} \leftrightarrow Ni^{4+}$ above it. Similar to Ni^{2+}, Co^{2+} is also electrochemically active and its appearance is most visible in the voltage curves of CS 3-1 spinel. The inset shows that the oxidation of this ion to Co^{3+} takes place at 4.735 V and reduction back to Co^{2+} occurs at 4.705 V.

The control LMN cathode reaches a first cycle discharge capacity of 130.5 mAh g^{-1} with a coulombic efficiency (QE) of 83%. In Co-doped LMNC, discharge capacity rises to 134.1 mAh g^{-1} and QE improves to 85.4%. The positive impact of cobalt addition might be based on dual use of electrochemically active elements. The discharge capacity is lowered to 124.6 mAh g^{-1} in Al-doped LMNA. Since Al^{3+} is not an electrochemically active ion, its use creates a dead weight in the lattice, thereby lowering specific lithium capacity of spinel material. On the other hand, QE in the first cycle reaches its highest value of 88.2% with LMNA cathode. As the origin of poor coulombic efficiency in high voltage spinel materials is partly due to undesired electrolyte oxidation over spinel surface, Al doping might be beneficial in reducing such side reactions.

The coin cells underwent overall 80 charge and discharge cycles and the discharge capacity, percentage capacity retention and QE numbers gathered from these cycles are plotted as a function of cycle number in Fig. 5a–c. Based on first and last cycle discharge capacities, the percentage capacity retention values of LMN, LMNC and LMNA spinels are 86.5%, 89.8% and 91.9%, respectively. A similar trend is also noticed in coulombic efficiency data as well. In summary, cobalt doping had the most positive effect in boosting lithium capacity and aluminum doping enhanced coulombic efficiency and capacity retention over extended cycling. In the light of these results, a core–shell structure

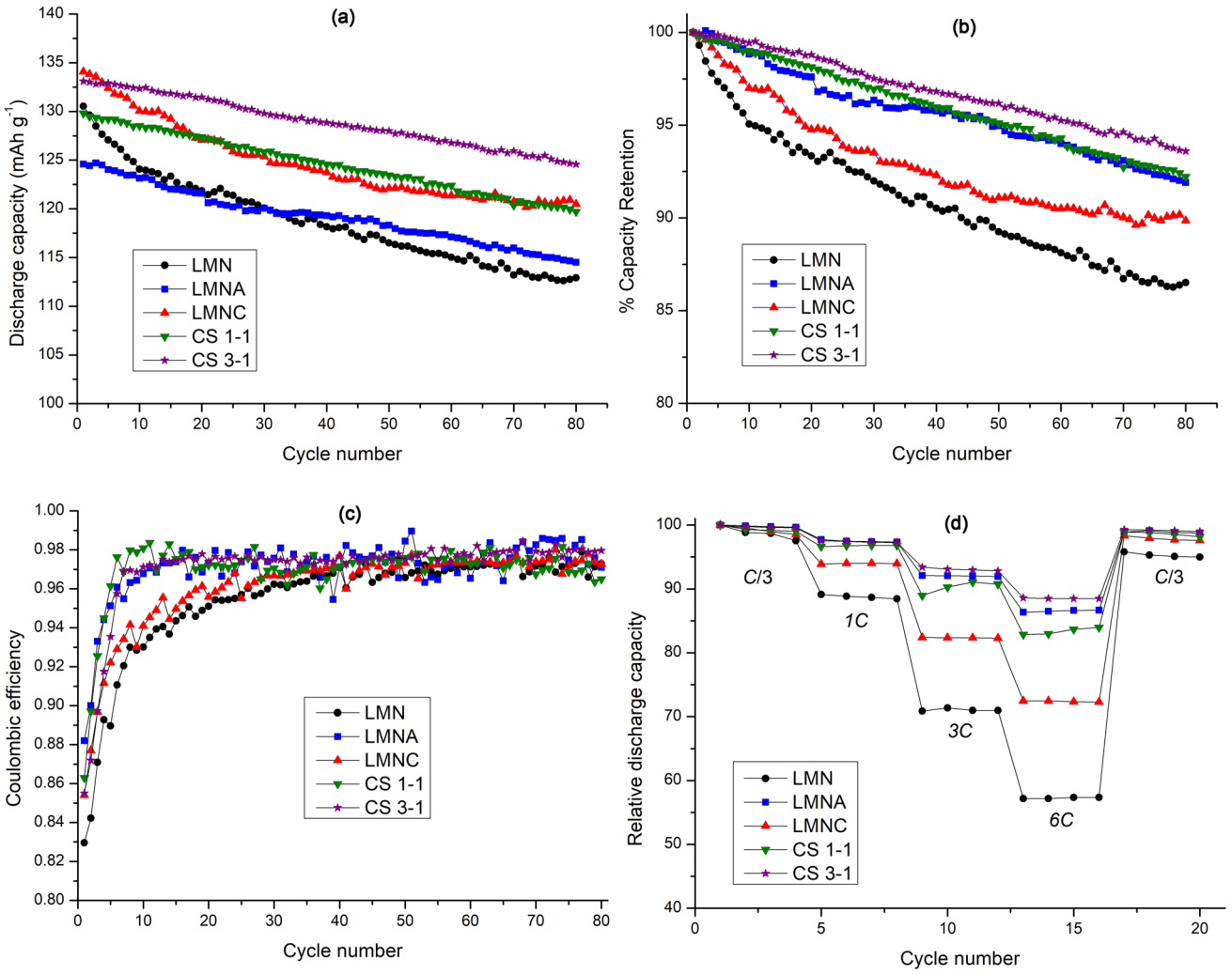

Fig. 5 Variation of **a** discharge capacities, **b** percentage capacity retention values and **c** coulombic efficiencies of five spinel cathodes with cycle number, **d** their normalized discharge capacities at different discharge rates

with Co-doped core and Al-doped shell was devised. This concept would create a synergetic coupling of LMNC and LMNA spinels with improved cathode behavior in all parameters. Specifically, the core of the material would be made of higher capacity spinel while the shell of the material offers increased protection against liquid electrolyte.

The core–shell-structured CS 3-1 and CS 1-1 cathodes have first cycle discharge capacities of 133.1 and 129.8 mAh g^{-1}, respectively. The lower discharge capacity of the latter is due to thicker outer LMNA shell. The first cycle coulombic efficiency is 85.5% for CS 3-1 and 86.3% for CS 1-1. These numbers are in close proximity of regular LMNA and LMNC spinels and better than control LMN cathode. The coulombic efficiency numbers of all five spinels stabilize around 97–98% on extended cycling. On the other hand, a significant improvement in the cyclability of spinel cathode is obtained with core–shell materials. The capacity loss after 80 cycles is reduced to 6.4% in CS 3-1 and 7.8% in CS 1-1 samples. The lowest fading rate attained with CS 3-1 corresponds to -0.08% loss per cycle. Even though, the percentage capacity retention values of both core–shell materials are slightly better than LMNA spinel, they also provide much larger lithium capacities. This fact proves that core–shell materials create a synergy and provide the best performance. Another point to be made is that the thickness of outer LMNA layer needs to be optimized since its excessive use hurts battery performance as observed with CS 1-1 spinel.

The rate capability of cathode materials were compared using sister cells. The cells were discharged at *C*/3, 1*C*, 3*C*, 6*C* and *C*/3 in sequence while spending 4 cycles at each current density. The charge current was kept *C*/3 at all times. The normalized capacities of five spinel materials with respect to *C*/3 rate are plotted in Fig. 5d. The Al-doped materials appear to have the best rate performance. Among the Al-doped electrodes, core–shell-structured CS 3-1 is the best and the distinction among CS 3-1, CS 1-1 and LMNA becomes more apparent at higher discharge current densities. On the other hand, undoped LMN exhibits the worst rate performance and LMNC lies in the middle. The ratio of the capacity at 6*C* to the one at *C*/3 is 0.80–0.88 in cases of Al-doped cathodes. The same numbers are 0.72 and 0.56 for LMNC and bare LMN, respectively. The positive effect of Al doping on the rate performance of $LiMn_{1.5}Ni_{0.5}O_4$ was reported previously [53]. The authors based this performance difference on improved electronic conductivity upon doping and morphological differences, citing higher interparticle boundary resistance in bare LMN. It was mentioned previously that the surfaces of Al-doped LMNA, CS 1-1 and CS 3-1 powders are much denser than those of LMN and LMNC powders. Such dense surface structure could possibly result in improved electronic and ionic conductivities in favor of Al-doped materials due to lesser degree of interparticle resistance. In order to confirm this, impedance spectroscopy analyses of cells were conducted at the end of rate protocol and their *Z*-plots are displayed in Fig. 6. The intercept at *Z*′ axis in high frequency corresponds to electrolyte resistance (R_e) and the semi circle in middle-to-low frequency range refers to charge transfer resistance (R_{ct}) of the solid electrode. It is seen unambiguously that Al-doped cathode materials have noticeably smaller R_{ct} than LMNC and LMN. Specifically, the R_{ct} is around 150 Ω for CS 3-1 and LMNA, 165 Ω for CS 1-1, 190 Ω for LMNC and 250 Ω for bare LMN. The positive correlation between rate capability and charge transfer resistance supports the above hypothesis that porous vs. dense surface morphology might account for the rate performance difference between cathode materials. Besides the morphological differences, the structural changes upon Al doping should also be considered as a source of impedance. It is known that the most outer 5–10 nm layer of cathode materials can undergo phase transformations due to atomic rearrangement of transition metals at high voltages, resulting in metal dissolution from cathode material [54]. Due to the higher strength of Al-O bonding, Al doping might help stabilize spinel lattice, thereby mitigating impedance growth.

4 Conclusion

$LiMn_{1.5}Ni_{0.5}O_4$(LMN) spinel is one of the most promising alternative lithium-ion battery cathodes owing to its reliance on cheap and abundant manganese ores as well as very easy synthesis requirements. In this study, we investigated the effect of Co and Al dopants on cathode performance and found out that the most notable contribution of cobalt was to increase discharge capacity while aluminum doping helped both cyclability and rate capability. By incorporating

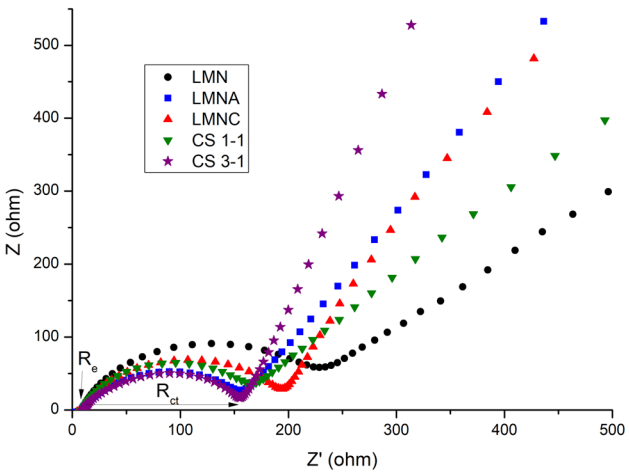

Fig. 6 *Z*-plots of five spinel electrodes

these two elements in a core–shell structure, a synergy was formed. This new material contained a bulk with larger lithium capacity and a surface with better stability. The core–shell materials exhibited better performance than control and individually doped spinel cathodes. Our future work will concentrate on the optimization of shell layer thickness and composition where the use of other elements such as B and Mg will be also explored.

Supplementary Information The online version contains supplementary material available at https://doi.org/10.1007/s10800-021-01653-y.

Acknowledgements This project received financial support from TUBITAK under the project number of 217M113 and from Tarsus University under the project number of HUBF.20.001.

References

1. Tan X, Zhang M, Li J, Zhang D, Yan Y, Li Z (2020) Recent progress in coatings and methods of Ni-rich $LiNi_{0.8}Co_{0.1}Mn_{0.1}O_2$ cathode materials: a short review. Ceram Int 46(14):21888–21901
2. Gao P, Wang S, Liu Z, Jiang Y, Zhou W, Zhu Y (2020) Experimental and mechanism research of gradient structured $LiNi_{0.8}Co_{0.1}Mn_{0.1}O_2$ cathode material for Li-ion batteries. Solid State Ionics 357:115504
3. Zhu L, Bao C, Xie L, Yang X, Cao X (2020) Review of synthesis and structural optimization of $LiNi_{1/3}Co_{1/3}Mn_{1/3}O_2$ cathode materials for lithium-ion batteries applications. J Alloys Compd 831:154864
4. Yan X, Zhang L, Lu J (2019) Improve safety of high energy density $LiNi_{1/3}Co_{1/3}Mn_{1/3}O_2$/graphite battery using organosilicon electrolyte. Electrochim Acta 296:149–154
5. Gao TP, Wong KW, Ng KM (2020) High-quality $LiNi_{0.8}Co_{0.15}Al_{0.05}O_2$ cathode with excellent structural stability: suppressed structural degradation and pore defects generation. Nano Energy 73:104798
6. Amin R, Muralidharan N, Petla RK, Yahia HB, Al-Hail SAJ, Essehli R, Daniel C, Khaleel MA, Belharouak I (2020) Research advances on cobalt-free cathodes for Li-ion batteries—the high voltage $LiMn_{1.5}Ni_{0.5}O_4$ as an example. J Power Sources 467:228318
7. Gargi G, Aklalouch M, Favotto C, Mansori M, Saadoune I (2020) Coprecipitation synthesis of Co-doped $LiMn_{1.5}Ni_{0.5}O_4$ material as 5 V cathode of Li-ion batteries with huge rate capability for high power applications. J Electroanal Chem 873:114413
8. Luo W (2015) Effect of morphology on the physical and electrochemical properties of the high-voltage spinel cathode $LiMn_{1.5}Ni_{0.5}O_4$. J Alloys Compd 636:24–28
9. Wu Q, Xue K, Zhang X, Xie X, Wang H, Zhang J, Li Q (2019) Enhanced cyclic stability at elevated temperature of spinel $LiNi_{0.5}Mn_{1.5}O_4$ by $Li_4Ti_5O_{12}$ coating as cathode material for high voltage lithium ion batteries. Ceram Int 45(4):5072–5079
10. Shin QW, Manthiram A (2011) Surface-segregated, high-voltage spinel $LiMn_{1.5}Ni_{0.42}Ga_{0.08}O_4$ cathodes with superior high-temperature cyclability for lithium-ion batteries. Electrochem Commun 13(11):1213–1216
11. Wei L, Tao J, Yang Y, Fan X, Ran X, Li J, Lin Y, Huang Z (2020) Surface sulfidization of spinel $LiNi_{0.5}Mn_{1.5}O_4$ cathode material for enhanced electrochemical performance in lithium-ion batteries. Chem Eng J 384:123268
12. Luo Y, Lu T, Zhang Y, Yan L, Mao SS, Xie J (2017) Surface-segregated, high-voltage spinel lithium-ion battery cathode material $LiNi_{0.5}Mn_{1.5}O_4$ cathodes by aluminium doping with improved high-rate cyclability. J Alloys Compd 703:289–297
13. Chong J, Xun S, Song X, Liu G, Battaglia VS (2013) Surface stabilized $LiNi_{0.5}Mn_{1.5}O_4$ cathode materials with high-rate capability and long cycle life for lithium ion batteries. Nano Energy 2(2):283–293
14. Zhang K, Li P, Ma M, Park JH (2016) Designed seamless outer surface: application for high voltage $LiNi_{0.5}Mn_{1.5}O_4$ cathode with excellent cycling stability. J Power Sources 336:307–315
15. Liu D, Bai Y, Zhao S, Zhang W (2012) Improved cycling performance of 5 V spinel $LiMn_{1.5}Ni_{0.5}O_4$ by amorphous $FePO_4$ coating. J Power Sources 219:333–338
16. Shi JY, Yi CW, Kim K (2010) Improved electrochemical performance of AlPO4-coated $LiMn_{1.5}Ni_{0.5}O_4$ electrode for lithium-ion batteries. J Power Sources 195(19):6860–6866
17. Zhu YR, Yi TF, Zhu RS, Zhou AN (2013) Increased cycling stability of $Li_4Ti_5O_{12}$-coated $LiMn_{1.5}Ni_{0.5}O_4$ as cathode material for lithium-ion batteries. Ceram Int 39(3):3087–3094
18. Yubuchi S, Ito Y, Matsuyama T, Hayashi A, Tatsumisago M (2016) 5 V class $LiNi_{0.5}Mn_{1.5}O_4$ positive electrode coated with Li_3PO_4 thin film for all-solid-state batteries using sulfide solid electrolyte. Solid State Ionics 285:79–82
19. Chae JS, Yoon SB, Yoon WS, Kang YM, Park SM, Lee JW, Roh KC (2014) Enhanced high-temperature cycling of Li_2O–$2B_2O_3$-coated spinel-structured $LiNi_{0.5}Mn_{1.5}O_4$ cathode material for application to lithium-ion batteries. J Alloys Compd 601:217–222
20. Bai N, Ma Y, Wang A, Luo X (2021) Effects of MoO_3 coating on the structure and electrochemical performance of high-voltage spinel $LiNi_{0.5}Mn_{1.5}O_4$. Ionics. https://doi.org/10.1007/s11581-020-03847-4
21. Pan JJ, Chen B, Xie Y, Ren N, Yi TF (2019) V_2O_5 modified $LiNi_{0.5}Mn_{1.5}O_4$ as cathode material for high-performance Li-ion battery. Mater Lett 253:136–139
22. Cabana J, Zheng H, Shukla AK, Kim C, Battaglia VS, Kunduraci M (2011) Comparison of the performance of $LiNi_{1/2}Mn_{3/2}O_4$with different microstructures. J Electrochem Soc 158:A997
23. Wei Y, Tuo K, Wang P, Li Y, Liang W, Ding H, Cui X, Li S (2021) Appropriate proportion of truncated octahedron $LiNi_{0.5}Mn_{1.5}O_4$ with excellent electrochemical properties for lithium-ion batteries prepared by graphite-assisted calcination method. Ionics 26:6003–6012
24. Tan C, Yang J, Pan Q, Li Y, Li Y, Cui L, Fan X, Zheng F, Wang H, Li Q (2021) Optimizing interphase structure to enhance electrochemical performance of high voltage $LiNi_{0.5}Mn_{1.5}O_4$ cathode via anhydride additives. Chem Eng J 410:128422
25. Luo X (2018) Improvement of the electrochemical performance of spinel $LiNi_{0.5}Mn_{1.5}O_4$ by stabilization of the electrode/electrolyte interfaces with the electrolyte additive. J Alloys Compd 730:23–30
26. Yang Y, Li S, Zhang Q, Zhang Y, Xu SM (2017) Agglomeration of octahedral $LiNi_{0.5}Co_{4x}Mn_{1.5\text{-}3x}O_4$ cathode material prepared by a continuous coprecipitation method for 5V lithium-ion batteries. Ind Eng Chem Res 56:75–182
27. Wang S, Li P, Shao L, Wu K, Lin X, Shui M, Long N, Wang D, Shu J (2015) Preparation of spinel $LiNi_{0.5}Mn_{1.5}O_4$ and Cr-doped $LiNi_{0.5}Mn_{1.5}O_4$ cathode materials by tartaric acid assisted sol-gel method. Cer Int 41:1347–1353
28. Luo Y, Lu T, Zhang Y, Yan L, Mao SS, Xie J (2017) Surface-segregated, high-voltage spinel lithium-ion battery cathode material $LiNi_{0.5}Mn_{1.5}O_4$ cathodes by aluminum doping with improved high-rate cyclability. J Alloys Compd 703:289–297
29. Wei A, Mu J, He R, Bai X, Liu Z, Zhang L, Wang Y, Liu Z (2021) Enhancing electrochemical performance and structural stability

of $LiNi_{0.5}Mn_{1.5}O_4$ cathode material for rechargeable lithium-ion batteries by boron doping. Ceram Int 47:226–237
30. Locati C, Lafont U, Simonin L, Ooms F, Kelder EM (2007) Mg-doped $LiNi_{0.5}Mn_{1.5}O_4$ spinel for cathode materials. J Power Sources 174:847–851
31. Yavuz NK, Yavuz M, Indris S, Bramnik NN, Knapp M, Dolotko O, Das B, Ehrenberg H, Bhaskar A (2016) Enhancement of electrochemical performance by simultaneous substitution of Ni and Mn with Fe in Ni-Mn spinel cathodes for lithium-ion batteries. J Power Sources 327:507–518
32. Zong B, Deng Z, Yan S, Lang Y, Gong J, Guo J, Wang L, Liang G (2020) Effects of Si doping on structural and electrochemical performance of $LiNi_{0.5}Mn_{1.5}O_4$ cathode materials for lithium-ion batteries. Powder Technol 364:725–737
33. Yi TF, Chen B, Zhu YR, Li XY, Zhu RS (2014) Enhanced rate performance molybdenum-doped spinel $LiNi_{0.5}Mn_{1.5}O_4$ cathode materials for lithium ion battery. J Power Sources 247:778–785
34. Zong B, Lang Y, Yan S, Deng Z, Gong J, Guo J, Wang L, Liang G (2020) Influence of Ti doping on microstructure and electrochemical performance of $LiNi_{0.5}Mn_{1.5}O_4$ cathode material for lithium-ion batteries. Mater Today Comm 24:101003
35. Feng S, Kong X, Sun H, Wang B, Luo T, Liu G (2018) Effect of Zr doping on $LiNi_{0.5}Mn_{1.5}O_4$ with ordered and disordered structures. J Alloys Compd 749:1009–1018
36. Li S, Wei Y, Wang P, Feng Y, Liang W, Ding H, Cui X (2020) Synergism of Cu and Al co-doping on improvements of structural integrity and electrochemical performance for $LiNi_{0.5}Mn_{1.5}O_4$. J Alloys Compd 820:153140
37. Lin F, Guo J, Wang L, Zhou Y, Wu H, Zhou D (2021) Synergistic effect of Mg and Y co-dopants on enhancement of electrochemical properties of $LiNi_{0.5}Mn_{1.5}O_4$ spinel. Electrochim Acta 399:139433
38. Shu X, Zhao H, Hu Y, Liu J, Tan M, Liu S, Zhang M, Ran Q, Li H, Liu X (2018) Magnesium and silicon co-doped $LiNi_{0.5}Mn_{1.5}O_4$ cathode material with outstanding cycling stability for lithium-ion batteries. Vacuum 156:1–8
39. Mao J, Dai K, Xuan M, Shao G, Qiao R, Yang W, Battaglia VS, Liu G (2016) Effect of chromium and niobium doping on the morphology and electrochemical performance of high-voltage spinel $LiNi_{0.5}Mn_{1.5}O_4$ cathode material. ACS Appl Mater Interfaces 8:9116–9124
40. Zheng X, Liu W, Qu Q, Zheng H, Huang Y (2019) Bi-functions of titanium and lanthanum co-doping to enhance the electrochemical performance of spinel $LiNi_{0.5}Mn_{1.5}O_4$ cathode. J Materiomics 5:156–163
41. Jeong M, Kim H, Lee W, Ahn SJ, Lee E, Yoon WS (2020) Stabilizing effects of Al-doping on Ni-rich $LiNi_{0.80}Co_{0.15}Mn_{0.05}O_2$ cathode for Li rechargeable batteries. J Power Sources 474:228592
42. Zhong GB, Wang YY, Zhang ZC, Chen CH (2011) Effects of Al substitution for Ni and Mn on the electrochemical properties of $LiNi_{0.5}Mn_{1.5}O_4$. Electrochim Acta 56:6554–6561
43. Kunduraci M, Amatucci GG (2007) Effect of oxygen non-stoichiometry and temperature on cation ordering in $LiMn_{2-x}Ni_xO_4$ ($0.50 \geq x \geq 0.36$) spinels. J Power Sources 165(1):359–367
44. Lee J, Dupre N, Avdeev M, Kang B (2017) Understanding the cation ordering transition in high-voltage spinel $LiNi_{0.5}Mn_{1.5}O_4$ by doping Li instead of Ni. Sci Reports 7:6728
45. Ariyoshi K, Iwakoshi Y, Nakayama Y, Ohzuku T (2004) Topotactic two-phase reactions of $Li[Ni_{1/2}Mn_{3/2}]O_4$ ($P4_332$) in non-aqueous lithium cells. J Electrochem Soc 151:A296–A303
46. Kim JH, Huq A, Chi M, Pieczonka NPW, Lee E, Bridges CA, Tessema MM, Manthiram A, Persson KA, Powell BR (2014) Integrated nano-domains of disordered and ordered spinel phases in $LiNi_{0.5}Mn_{1.5}O_4$ for Li-ion batteries. Chem Mater 26(15):4377–4386
47. Kunduraci M, Al-sharab JF, Amatucci GG (2006) High-power nanostructured $LiMn_{2-x}Ni_xO_4$ high-voltage lithium-ion battery cathode: electrochemical impact of electronic conductivity and morphology. Chem Mater 18(15):3585–3592
48. Xiao J, Yu X, Zheng J, Zhou Y, Gao F, Chen X, Bai J, Yang XQ, Zhang JG (2013) Interplay between two-phase and solid solution reactions in high voltage spinel cathode material for lithium ion batteries. J Power Sources 242:736–741
49. Liu G, Park KS, Song J, Goodenough JB (2013) Influence of thermal history on the electrochemical properties of $Li[Ni_{0.5}Mn_{1.5}]O_4$. J Power Sources 243:260–266
50. Zeng F, Zhang Y, Shao Z, Li Z, Dai S (2021) The influence of different calcination temperatures and times on the chemical performance of $LiNi_{0.5}Mn_{1.5}O_4$ cathode materials. Ionics 27:3739–3748
51. Lin B, Yin Q, Hu H, Lu F, Xia H (2014) $LiMn_2O_4$ nanoparticles anchored on graphene nanosheets as high-performance cathode material for lithium-ion batteries. J Solid State Chem 209:23–28
52. Terada Y, Yasaka K, Nishikawa F, Konishi T, Yoshio M, Nakai I (2001) In situ XAFS analysis of $Li(Mn, M)_2O_4$ (M = Cr Co, Ni) 5V cathode materials for lithium-ion secondary batteries. J Solid State Chem 156(2):286–291
53. Sun P, Ma Y, Zhai T, Li T (2016) High performance $LiNi_{0.5}Mn_{1.5}O_4$ cathode by Al-coating and Al^{3+}-doping through a physical vapor deposition method. Electrochim Acta 191:237–246
54. Kim CA, Choi HJ, Lee JH, Yoo SY, Kim JW, Shim JH, Kang B (2015) Influence of surface modification on electrochemical performance of high voltage spinel ordered-$LiNi_{0.5}Mn_{1.5}O_4$ exposed to 5.3 V for 100 h before and after surface modification with ALD method. Electrochim Acta 184:134–142

Authors and Affiliations

Muharrem Kunduraci[1] · Uğur Çağlayan[2]

[1] Department of Aerospace Engineering, Tarsus University, Mersin, Turkey

[2] Central Research Laboratory, Cukurova University, Adana, Turkey